NASA Technical Memorandum 104498

Solar Dynamic Modules for Space Station Freedom: The Relationship Between Fine-Pointing Control and Thermal Loading of the Aperture Plate

Roger D. Quinn
Case Western Reserve University
Cleveland, Ohio

and

Thomas W. Kerslake
Lewis Research Center
Cleveland, Ohio

Prepared for the
International Solar Energy Conference
sponsored by the American Society of Mechanical Engineers
Lahaina, Maui, Hawaii, April 5-9, 1992

NASA

SOLAR DYNAMIC MODULES FOR SPACE STATION FREEDOM: THE RELATIONSHIP BETWEEN FINE-POINTING CONTROL AND THERMAL LOADING OF THE APERTURE PLATE

Roger D. Quinn*
Case Western Reserve University
Department of Mechanical & Aerospace Engineering
Cleveland, Ohio 44106

Thomas W. Kerslake
National Aeronautics and Space Administration
Lewis Research Center
Cleveland, Ohio 44135

E-6109

SUMMARY

Dynamic simulations of Space Station Freedom configured with SD power modules were performed. The structure was subjected to shuttle docking disturbances, while being controlled with a "natural" vibration and tracking control approach. Three control cases were investigated for the purpose of investigating the relationship between actuator effort, SD pointing and thermal loading on the receiver aperture plate. Transient, one-dimensional heat transfer analyses were performed to conservatively predict temperatures of the multi-layered receiver aperture plate assembly and thermal stresses in its shield layer. Results indicate that the proposed aperture plate is tolerant of concentrated flux impingement during short-lived structural disturbances. Pointing requirements may be loosened and the required control torques lessened from that previously specified. Downsizing and simplifying the joint drive system should result in a considerable savings in mass.

INTRODUCTION

This paper addresses the problem of fine-pointing (aligning) the concentrator-receiver-sun system of the proposed Solar Dynamic (SD) power modules for Space Station Freedom. The purpose is to show the relationship between fine-pointing control effort and thermal loading on the receiver aperture plate in terms of fine-pointing precision.

Freedom's initial power source is to be photovoltaic but SD is essential for growth. Freedom configured with SD power systems is illustrated in figure 1. This growth configured Freedom model (MB15) incorporates eight photovoltaic (PV) arrays and two SD modules. A view of an SD power module is shown in figure 2. The concentrator collects and focuses the sun's radiated energy through an aperture into the receiver and, thus, provides the heat energy input for a Closed Brayton Cycle power system. The SD power system is described in detail by Secunde et al. [1].

The pointing/heating relationship is crucial for establishing fine-pointing precision requirements, especially off-pointing limits. More strict pointing specifications require greater control

---

*Summer Faculty Fellow at NASA Lewis Research Center.

effort, larger controlling motors and/or more complicated transmissions and control procedures, all with weight and maintenance penalties. Loose pointing specifications lead to off-pointing and associated power output losses and extensive thermal loading of the aperture plate. The Freedom configuration shown in figure 1 is a multibody dynamical system. Its control systems include space station attitude and reboost controllers and for the outboard truss power modules control systems: (1) an Alpha joint in the truss to permit orbital sun tracking about the y axis (truss longitudinal axis), (2) a Beta joint between each power module and the truss to permit rotation about an axis normal to the truss for seasonal sun tracking, and (3) two axis joints for fine-pointing (FP) the SD concentrator relative to the sun and relative to the receiver aperture. SD pointing requires alignment of the system consisting of the sun, concentrator, and receiver aperture.

Freedom's structure is rather flexible with natural frequencies below one-tenth of a Hz. There has been concern that this structural flexibility might limit the SD fine-pointing control precision. This concern sparked the pointing control versus aperture plate heating research which is presented in this paper.

A control approach was developed for multibody space structures like Freedom where both large, rigid-body motions and vibratory motions are controlled using the same hardware [2]. In this way, SD modules can be targeted and fine-pointed while, simultaneously, structural vibrations are damped. This control system is robust to control/structure interactions that might lead to instability. Controller effort is strongly related to pointing precision and the control method. This paper investigates the feasibility of this control approach in light of thermal limits. A NASTRAN structural dynamics model developed by the NASA Lewis Research Center Engineering Directorate is used to simulate the motions of Freedom during dynamic disturbances and to demonstrate the control approach.

The receiver aperture plate assembly, described briefly in [3], is illustrated in figure 3. The assembly is comprised of four layers: (1) graphite segments, (2) Haynes Alloy 188 (HA 188) plate, (3) Multi-Foil Insulation (MFI), and (4) refractory board insulation. The graphite, MFI and board insulation layers are mechanically attached to the HA 188 plate in a loose-fitting manner to accommodate differential thermal expansion of the layers. Temperature limits for these materials are given in table I. The aperture plate assembly fulfills three primary requirements: (1) reduction in radiative heat loss from the receiver cavity, (2) protection of receiver hardware during concentrator off-pointing events, and (3) enhancement of receiver structural rigidity for ground and/or flight operations and handling.

The second requirement, to protect receiver hardware during concentrator off-pointing events, is unquestionably the most challenging requirement due to the high fluxes (100's of W/cm^2) which must be tolerated during off-pointing. The same requirement also exists for terrestrial solar heat receivers. Experiments were conducted to determine the capability of various materials to provide protection from high solar fluxes [4]-[6]. Results from these experiments showed that a medium grain size (nominal particle size < 750 μm) graphite performed well under high flux loadings [5].

Several heat transfer analyses of aperture plate materials have also been conducted. In [7], a one-dimensional analysis of a single zirconium dioxide board confirmed experimental temperature data which revealed that the material was partially transparent to solar wavelength radiation. The solar transparency led to infrared radiation "trapping" which caused maximum temperatures at the board mid-thickness instead of at the surface of flux impingement. A

two-dimensional analysis of a single graphite, copper, or quartz plate undergoing a solar beam off-pointing event was conducted in [8]. Temperature variations through the plate thickness were not considered. Temperatures exceeded 3000 K along the solar beam off-pointing path (with a 2-mrad slope error concentrator). Results indicted that graphite is a promising high flux protection material. In [9], a one-dimensional analysis was conducted of adjacent graphite-HA 188 layers during a controlled, 3-sec duration solar off-pointing (detrack). Results showed that relatively low temperatures (i.e., ~1200 K) occurred as a consequence of this brief detrack event.

In this paper, a one-dimensional analysis of the multi-layered aperture plate assembly shown in figure 3 is performed to determine temperature distributions within each layer and the heat transfer between adjacent layers. This approach, which is unlike those listed above, is necessary to enable the calculation of thermal stresses and to capture the nature of energy diffusion through the various layers over the duration of extended (i.e., 100's or 1000's of seconds) heating transients due to off-pointing. In addition, material durability calculations were performed to assess the ability of the aperture plate design to withstand thermal stresses and material loss through sublimation.

High-flux, solar heating transients are caused by concentrator pointing disturbances which occur following a space shuttle orbiter docking with Freedom. The concentrator off-pointing responses for three different SD module fine-pointing control situations denoted Cases I, II, and III, are examined for the purpose of developing a relationship between fine-pointing control effort and thermal loading of the aperture plate assembly. The relationship between control effort and thermal loading/system power output can be used in an overall system cost analysis and trade-off study for future designs. The results may permit fine-pointing specifications and aperture plate thermal design specifications to be chosen in a consistent and reliable fashion.

STRUCTURAL DYNAMIC MODEL

Space Station Freedom is a multibody dynamic system. A NASTRAN structural model of the Freedom growth configuration (MB15 with SD) shown in figure 1 was developed by the NASA Lewis Research Center Engineering Directorate. This model includes laboratory modules, low modulus truss, eight photovoltaic (PV) arrays and two SD modules.

The many thousands of degrees of freedom were reduced through modal ordering to 149 modes which were found to have the most pronounced effects on the SD modules. The model includes 22 rigid-body modes: 6 for the main modules and truss; 2 provided by the Alpha joints; 10 provided by the PV and SD Beta joints; 4 provided by the SD FP joints. The balance is a set of 127 flexible structural system modes. Table II contains the first 38 flexible mode natural frequencies in ascending order. Note the repeated frequencies in sets of eight which correspond to the PV arrays. The SD radiator has a strong participation in some of the lowest modes. The concentrator support assembly is relatively stiff. Its cantilevered natural frequency is reported to be at about 1.6 Hz.

In nominal operation the main structure (inside the Alpha joints) rotates to maintain its attitude relative to the Earth throughout its orbit on the order of 0.0002 Hz (Alpha rotation rate). The Alpha and Beta joints rotate at orbital and seasonal frequencies, respectively, such that the orientations of the SD and PV modules remain fixed relative to the Sun.

The external disturbances which appear to have the most pronounced effects on the pointing of SD modules are aerodynamic drag and shuttle docking (or berthing). During docking, the shuttle interacts structurally with the station and its control jet-plumes impinge on the station. Aerodynamic drag and the gravity gradient apply loads which vary at the orbital frequency. This frequency is two orders of magnitude slower than the structural frequencies and so can be considered relatively constant. With integral control these disturbances should not cause undue pointing problems, given motors with the necessary torque capacity. Shuttle docking applies transient dynamic disturbances which may excite the structural modes of vibration. For this reason, there has been concern that docking may cause pointing difficulties.

The NASTRAN finite element model of the distributed parameter space station can be expressed by the following discrete equations of motion in matrix form:

$$M \ddot{\underset{\sim}{x}} + C \dot{\underset{\sim}{x}} + K \underset{\sim}{x} = \underset{\sim}{F} \tag{1}$$

where M, C, and K are the N x N mass, damping and stiffness matrices and $\underset{\sim}{F}$ and $\underset{\sim}{x}$ are the N x 1 force and displacement vectors. Actually, C is assumed to be proportional to the K matrix, so that the damped and undamped eigenvectors are identical.

Through modal ordering a subset X (N x n) of the modal matrix which includes those eigenvectors that contribute the most to the motion of the SD modules is formed. This permits the motion of Freedom to be approximated as

$$\underset{\sim}{x} \cong X \underset{\sim}{\eta} \tag{2}$$

The reduced-order model in natural or modal coordinates $\underset{\sim}{\eta}$ can be expressed in scalar form as

$$\ddot{\eta}_i + 2 \zeta_i \omega_i \dot{\eta}_i + \omega_i^2 \eta_i = f_i \qquad i = 1, 2, \ldots, n \tag{3}$$

where ω_i and ζ_i are the natural frequency and damping ratios of the ith mode, respectively. The modal forces $\underset{\sim}{f}$ are related to the physical forces $\underset{\sim}{F}$ by the following equation:

$$\underset{\sim}{f} = X^T \underset{\sim}{F} \tag{4}$$

The modal and physical forces can be partitioned into two parts: control forces and disturbance forces or $\underset{\sim}{f} = \underset{\sim}{f}_c + \underset{\sim}{f}_d$ and $\underset{\sim}{F} = \underset{\sim}{F}_c + \underset{\sim}{F}_d$. The actuators are capable of applying a limited torque at the joints relative to the adjacent bodies. The actuator torques are transformed to modal forces through equation (4) for control gain design and for dynamic simulation.

VIBRATION AND TRACKING CONTROL SYSTEM

Freedom is a collection of flexible bodies connected by joints with actuators at the joints. The actuators couple the various rigid-body modes of Freedom through the joints. The flexible modes are also coupled so that all the closed-loop modes can be altered substantially from their open-loop form. Hence, the control system reduces the number of rigid-body modes from 22 to 6.

When the sensors are collocated with the actuators and PD control laws are used, the actuators act as springs and dampers at the joints. This "natural control" strategy precludes undesirable control/structure interactions and provides desirable vibration damping to the structure.

Tracking (e.g., the SD module tracking the sun while the main station remains Earth-oriented) requires relative rigid-body motions and can be achieved using inertial navigation sensors such as Sun sensors. The inertial information can be fed back to the collocated joint controller so that the effective null "stretch length" of the "active spring" changes accordingly. With this in mind, the feedback control torque for a joint can be expressed as

$$\tau = -k\left(\theta - \theta_o\right) - c\left(\dot{\theta} - \dot{\theta}_o\right) - I\int\left(\theta - \theta_o\right)dt \tag{5}$$

θ_o and $\dot{\theta}_o$ are the desired joint relative angular displacement and velocity which vary at the orbital rate. θ and $\dot{\theta}$ are the measured relative joint angular displacement and velocity. The control gains (k, c, and I) may remain constant or may be chosen to be time-varying based on rigid-body motions. The tracking (and, hence, time rate of change of θ_o and $\dot{\theta}_o$) will be at a relatively slow rate (90 min orbital period) compared to the structural frequencies and vibration controller frequencies.

This "natural" control approach is discussed in detail in [2] along with the dynamic simulation method. The control gains were chosen based on the desired rigid-body performance. With this type of control there is beneficial spillover into the flexible modes which attenuates the vibrations of station.

Dynamic Simulations of Freedom

Numerical simulations of Freedom were conducted to relate control effort with SD pointing precision during shuttle docking. The input docking forces and moments (Figs. 4 and 5) are the worst case of those developed by NASA Johnson Spaceflight Center Loads and Structural Dynamics Branch. Structural damping is neglected. Three cases are presented. In each case the model and disturbance (docking) are the same, but the controllers are different. Table III is a summary of the three cases. In each case the rigid-body design controller bandwidths for station attitude were chosen as 0.01 Hz and for the Alpha joints, PV Beta joints and SD Beta joints the design bandwidths were chosen as 0.04 Hz. These values were chosen to be consistent with accepted values from past work.

Case I

In Case I, the rigid-body design controller bandwidths for the FP joints were chosen as 0.5 Hz to be consistent with past work. The inertial concentrator orientation relative to the Sun is fed back directly to the FP joint controllers. Figure 6 shows the concentrator angular pointing errors and figure 7 shows the required SD Beta and FP control torques. The maximum off-pointing error is about 0.05° (9E-04 radians) and the maximum FP control torque is 2500 in.-lb (282.5 N-m). Note that the z angle represents rotation of the concentrator about a normal to the Sun. Hence, this angle does not affect pointing.

Case II

In Case II, the rigid-body design controller bandwidth for the FP inner joint was chosen as 10 percent of the previous value or 0.05 Hz. The outer FP joint was locked. The SD Beta joint was used for pointing in place of the outer FP joint in this case and in Case III. In Cases II and III the station inertial navigation system was used to sense the concentrator orientation and all joints were controlled with the tracking strategy of equation (5). The concentrator orientation was approximated by summing the station inertial orientation with the Alpha and Beta joint relative orientations. This measure is in error because the structural vibration is not taken into account. Figures 8 and 9 show the pointing angular errors and the torque requirements. The maximum error was 0.23° (0.004 radians) and the maximum torque required for pointing was 1000 in.-lb (113.0 N-m).

Case III

Case III is the same as Case II, except that in Case III the torques for all joints were limited to values which are representative of baseline design criteria. The torque limits are 7200 in.-lb (813.5 N-m) for station attitude, 1500 in.-lb (169.5 N-m) for Alpha joints, and 250 in.-lb (28.25 N-m) for all Beta joints and inner FP joints. Figures 10 and 11 show the pointing error and control torque histories. The maximum off-pointing error was 0.34° (0.006 radians). Note that the FP inner gimbal torque was clipped at the 250 in.-lb (28.25 N-m) limit.

APERTURE PLATE HEATING ANALYSIS

Input Solar Fluxes

The pointing disturbances discussed in the previous section create a two-dimensional solar image on the aperture plate which translates back and forth in the x and y directions while also rotating about z, the aperture plate surface normal. While the latter does not markedly affect the solar image, x and y translations cause significant image distortion and intensity reductions as shown in figure 12 (from [10]) for discrete pointing errors along the x-direction. Essentially identical optical distortions also occur for pointing errors in the y-direction.

As a simplifying assumption, only the x component of image translation was considered for the thermal analyses. This assumption is conservative because single component image translations cause less defocusing and, thus, have higher associated flux levels. The single aperture plate location, at the upper aperture edge as shown in figure 12, was selected to

evaluate the time-dependent, incident flux boundary condition. (This is required due to the one-dimensional, "through-the-thickness" nature of the aperture plate assembly thermal model which does not accommodate spatial flux variations.) Solar fluxes are highest at this location so that temperature levels at all other locations should be less severe.

The data from [10] were used in two ways: (1) the time-dependent flux value at the location of interest is directly used (peak flux assumption) and (2) the area-integrated power impinging on the aperture plate is divided by the illuminated area to generate a time-dependent average flux input value for the location of interest (average flux assumption). The peak flux assumption implicitly assumes lateral energy transfer cannot occur within aperture plate layers and thus, temperature predictions will be conservative. Conversely, the average flux assumption implicitly assumes an infinite ability for lateral energy transfer (over the illuminated area) and hence, nonconservative temperature levels will be predicted. However, in this paper conservative temperature predictions, i.e., employing the peak flux assumption, are presented. These predictions are then discussed in light of results obtained using the average flux assumption.

Aperture Plate Assembly Heat Transfer

A transient, one-dimensional heat transfer analysis of the aperture plate assembly was performed. Within the solid layers, the heat diffusion equation was solved. Within the MFI layer (the layer which exhibits the highest thermal resistance), radiative energy transfer was solved using the following equation from [11]:

$$q = \frac{\sigma\left(T_i^4 - T_j^4\right)}{1/\epsilon_i + 1/\epsilon_j - 1 + \sum_{n=1}^{NF}\left[1/\epsilon_{n_i} + 1/\epsilon_{n_j} - 1\right]} \tag{6}$$

where q is the heat flux, in W/cm^2, T is the temperature, in K, σ is the Stefan-Boltzmann constant, ϵ is the emittance and where i and j are two plane surfaces separated by NF foils. For these analyses, NF was chosen to be 50 and the foils were assumed to have the same emittance on both surfaces, hence $\epsilon_{n_i} = \epsilon_{n_j} = \epsilon_f$.

Since the aperture plate layers are loose fitting and operate in a vacuum, thermal radiation is the predominate mode of heat transfer between layers. This radiative heat transfer is also described by equation (6) (which is valid for diffuse or specular surfaces) when NF is set to zero and when i and j denote the respective aperture plate layer surfaces of interest.

Thermal boundary conditions were applied to the front graphite surface facing the concentrator and to the back insulation board surface facing the internal receiver cavity wall. On the front surface, a time-dependent incident solar flux was applied and radiative exchange occurred with the space sink at a constant temperature of 255 K. The back surface exchanged radiation with the receiver cavity wall (constructed of HA 188) at a constant temperature of 1106 K. Due to potentially large temperature variations, temperature-dependent material properties were used. In addition, the MFI material density was adjusted to represent the average layer density. The adjustment factor equals the foil thickness (0.00127 cm) divided by the foil spacing (0.01524 cm), i.e., 1/12th.

Material Durability Calculations

Graphite segment in-plane thermal stresses were calculated assuming the segment was free of surface traction forces and that temperature varied only through the thickness of the segment. These are fairly good assumptions as long as: (1) the graphite segments have compliant supports and are free to expand differentially from the HA 188 plate, (2) no diffusion bonding occurs between the graphite segments and the HA 188 plate, and (3) the concentrated solar image remains well focused, i.e., for mispointing angles less than about 1.0°, which validates the use of one-dimensional aperture plate thermal modeling. From [12], the in-plane (IP) or lateral thermal stresses in the bulk material, subject to the aforementioned restrictions, are given by:

$$\sigma_{IP} = \frac{\alpha E}{1 - \upsilon}\left\{ - T + \frac{1}{2h}\int_{-h}^{h} T\, dz + \frac{3z}{2h^3}\int_{-h}^{h} Tz\, dz \right\} \tag{7}$$

where z is the coordinate through the graphite segment thickness 2h, E is Young's modulus, α is the coefficient of thermal expansion, ν is Poisson's ratio, and the temperature T is a function of z or T = T(z). Local material stresses, however, could be considerably larger due to inclusions or other material defects that act as stress risers. Because of this possibility, a premium grade of graphite should be specified for the aperture plate segments to reduce the likelihood of unexpected thermal shock cracking. UCAR grade ATJ graphite properties were used in the analysis.

Graphite sublimation losses were estimated using the Knudsen-Langmuir equation and the predominate vapor specie was assumed to be triatomic carbon. The graphite surface recession rate, in cm/sec, is given by:

$$\dot{s} = (\gamma P/\rho)(2\pi RT/M)^{-1/2} \tag{8}$$

where the evaporation coefficient γ, is taken as 1.0, R is the universal gas constant, M is the molecular weight, P is the vapor pressure, and ρ is the density. The surface recession rate was then integrated over time to determine the graphite thickness losses due to concentrator pointing disturbances and due to orbital spillage flux.

Another important material durability issue is low Earth orbit atomic oxygen (AO) chemical attack and erosion. Although not addressed in this paper, AO attack should be considered in selecting the appropriate graphite segment thickness. Data from [13], when adjusted to Space Station Freedom orbital altitudes, show graphite experiences a surface recession rate of about 0.007 cm/year when exposed to ram AO. Hence, only about 15 percent of the graphite segment thickness, in the worst possible case (i.e., constant ram AO exposure as opposed to a more realistic "sweeping" ram) would be lost in 30 years of operation. In addition, the long-term chemical compatibility of adjacent aperture plate layers must also be considered when assessing material durability.

Numerical Methods

The equations governing heat transfer were discretized and then solved using an explicit, finite-difference method. The aperture plate model finite-difference control volumes are shown in figure 13. The size and number of control volumes were chosen based on engineering judgment. The numerical time step selected, 0.05 sec, satisfied stability requirements and represented the value, below which, improvements in the numerical energy balance were negligible. In general, an energy balance was maintained to within one-tenth of 1 percent.

Graphite numerical temperature predictions were curve-fitted to a second-order polynomial to determine T(z) used in equation (7). Terms on the right hand side of equation (7) were integrated by hand and numerically evaluated to determine the thermal stresses at specified time increments. Graphite sublimation rates were determined at each time step and then summed over time to determine total thickness losses.

APERTURE PLATE HEATING RESULTS

Temperature Predictions

Aperture plate temperature predictions versus time for Cases I through III are shown in figure 14. Refer to figure 13 for finite-difference element numbers and their corresponding locations within the aperture plate assembly shown in figure 3. The Case I concentrator pointing disturbance is so slight that nominal pointing requirements are maintained and the peak flux is limited to 23 W/cm^2. Hence, figure 14(a) simply shows the nominal layer temperature variations through a 91-min Space Station Freedom orbit. Due to the excellent insulating characteristics of the MFI layer, the graphite and HA 188 operate at essentially the same temperature throughout the orbit reaching a maximum temperature of 1387 K. In this case, the maximum HA 188 and nickel temperatures both exceed the loosely defined maximum usage temperatures by about 20 K. However, with the average flux assumption, solar heating rates are so low that the overall temperature gradient through the aperture plate layers is reversed: that is, the graphite and HA 188 layers operate 200 to 350 K below the average receiver cavity temperature of 1106 K.

Case II temperature predictions versus time are shown in figure 14(b). The graphite temperature response closely follows the damped-sinusoidal concentrator pointing disturbance which lasts for about 1 min and produces a peak incident flux of 123 W/cm^2. A maximum graphite temperature of 1495 K is attained at 0.333 min. The temperatures of other aperture plate layers change only slightly from their near-steady, orbital operating values during insolation. With the average flux assumption, the magnitude of flux variation is small enough that graphite temperatures also remain essentially unchanged from their near-steady, orbital values during insolation of 886 K.

Case III temperature predictions versus time are shown in figure 14(c). In this case, the concentrator oscillates steadily for three cycles producing peak incident flux levels of 312 W/cm^2 after which the disturbance decays over a period of about 1 min. Again, the graphite temperature response closely follows that of the concentrator pointing disturbance. A maximum graphite temperature of 1994 K is reached at 0.8 min, the peak of the third undamped oscillation. The maximum HA 188 temperature reaches 1657 K at 1.567 min, 82 K above the solidus temperature for this alloy. At this time, the HA 188 and graphite are at the same temperature.

Thereafter, the graphite no longer irradiates the HA 188 but instead, behaves as a sink for radiative cooling. Temperature changes in the MFI and board insulation are insignificant indicating the near-adiabatic performance of the MFI. With the average flux assumption, however, excursions in temperature from near-steady, orbital values during insolation are very small for all layers. In this case, the largest temperature changes take place in the graphite layer with 15 K variations about an average 894 K temperature.

Design Modifications To Reduce Temperatures

Figure 15 illustrates aperture plate temperature gradients at various times for the Case III pointing disturbance. The maximum graphite temperature is reached at 0.8 min and the maximum HA 188 temperature occurs at about 1.5 min. Low heat transfer rates through the MFI cause the HA 188 to rapidly heat as graphite temperatures rise in response to the incident solar flux. Yet, at the same time, the MFI stabilizes the temperature of the board insulation. Therefore, it would be beneficial to switch the positions of the HA 188 and MFI within the aperture plate assembly to protect the HA 188 from high temperatures. The MFI material would then have to be changed to a temperature-resistant, refractory metal. Tungsten appears to be a good choice of foil material due to its high melting point, low emittance, and availability in MFI product form.

The heat transfer model of the baseline aperture plate assembly, shown in figure 3, was modified by switching the HA 188 and MFI layer positions and replacing the nickel MFI material with tungsten. All other model features and input data were held fixed. The thermal response of the modified aperture plate design to the Case III pointing disturbance was then analyzed employing the peak flux assumption. Results showed that the HA 188 operated at a constant 1113 K throughout the pointing disturbance while maximum graphite temperatures were essentially the same as those predicted for the baseline aperture plate design. In this case, all material layers operated well within their respective maximum usage temperature limits. The mass increase associated with using tungsten is 17 kg which represents a 12-percent increase in total aperture plate assembly mass.

A second design modification to reduce temperatures consisted of changing the aperture plate geometry from planar to conical. By employing a truncated cone section around the aperture periphery, the flux incident on the graphite segments is reduced by a factor equal to the cosine of the cone angle. Although reflected solar rays from the concentrator are not unidirectional, it is assumed that the cosine rule holds true on the average for the incident solar image. Analysis of the baseline aperture plate design, modified with a 45° cone angle, shows that Case III maximum graphite and HA 188 temperatures are reduced by 248 and 191 K, respectively. The mass increase associated with the truncated cone is 8.7 kg or equivalently, a 6-percent increase in total aperture plate assembly mass.

Material Durability

Figure 16 shows graphite segment thermal stresses versus time after orbiter docking for Case III. The in-plane stresses oscillate between tensile and compressive values as a function of the applied solar heating. At the outer and inner segment faces, a maximum compressive stress of 6.28 MPa is reached. This compares with a 66 MPa compressive strength in the appropriate temperature range. At the segment mid-plane, a maximum tensile stress of 3.14 MPa is reached.

This compares with a 31 MPa tensile strength in the appropriate temperature range. If required, the graphite segment thickness could be doubled (to account for higher than expected operational material loss) with only a 37-percent increase in stress levels. These bulk material stress levels are a factor of 7 to 10 below the material strength properties. Therefore, subject to the scope and assumptions of this structural analysis, thermal stresses should not represent a design limitation.

Graphite sublimation losses were calculated for Cases I and III. In both cases, the surface losses were negligible: that is, the graphite surface receded 2.9×10^{-10} cm for Case I (a typical 91-min orbit) and 3.4×10^{-8} cm for Case III (several minute mispointing transient following an orbiter docking). Assuming an average of six orbiter dockings each year, the integrated graphite surface loss over 30 years of Space Station Freedom operation, is only 5.6×10^{-5} cm. This surface loss is negligible especially when compared to the probable AO erosion surface loss which is three orders-of-magnitude greater.

SUMMARY AND CONCLUSIONS

Structural dynamic simulations were conducted using a NASTRAN finite element model of a growth configuration of Freedom. The station was subjected to forces and moments which are characteristic of those expected during shuttle docking. The station's attitude and its joints were controlled using a "natural" control approach where the actuators serve as active springs and dampers. Three control cases were investigated for the purpose of establishing a general relationship between actuator effort and SD pointing.

In Case I, pointing was maintained within nominal specifications (0.1°) during docking but required much control effort. In Case III, all the controllers were limited to torques which are representative of baseline values. FP control torque was limited to one-tenth of the value required in Case I while the resulting maximum off-pointing angle was about seven times that of Case I.

Transient, one-dimensional heat transfer analyses were conducted to conservatively predict aperture plate assembly temperatures for each case. The thermal analyses showed that HA 188 and nickel MFI material temperature limits were exceeded during the pointing disturbance in each case. However, by relaxing the conservative peak flux assumption, material temperature limits were no longer exceeded. Further reductions in HA 188 temperatures were demonstrated through aperture plate assembly design modifications. Graphite segment thermal stresses were calculated and found to be well within material structural allowables. In addition, graphite sublimation losses were shown to be negligible.

Taken as a whole, these results suggest that the aperture plate assembly will be tolerant of short-lived (on the order of minutes) pointing disturbances. Furthermore, relaxation of fine-pointing requirements consistent with Case III examined herein, is not only possible but also desirable to reduce the mass and complexity of the fine-pointing control system. For example, in Case III the outer FP gimbal is not used for pointing and can be eliminated. Instead, the SD Beta was used for FP control along with the inner FP gimbal. The lower FP control bandwidth permits this simplification.

Specific recommendations for further study are given below:

1. Follow the recommendations given in [5] and [6] to use a medium grain size, high quality graphite material. The graphite should be appropriately segmented to reduce thermal stresses and of a thickness compatible with anticipated material AO erosion losses (perhaps in the 1 to 2 cm range). Graphite's high-temperature, high-flux tolerance and low density make it ideally suited for a space-based solar receiver application.

2. Support aperture plate assembly layers loosely to permit unconstrained differential thermal expansion and preclude large thermal stresses.

3. Interchange the HA 188 and MFI layer positions and replace the nickel MFI material with a temperature-resistant refractory metal. Tungsten is a good refractory metal choice on the basis of desirable material properties and availability.

4. Employ a conical geometry, instead of a planar geometry, around the aperture to reduce maximum material temperatures. A 45° cone angle seems to be a reasonable design choice.

5. Verify the aperture plate assembly design performance by conducting detailed, three-dimensional thermal-structural analyses and on-sun testing.

REFERENCES

1. Secunde, R.; Labus, T.L.; and Lovely, R.G.: Solar Dynamic Power Module Design. Proceedings of the 24th International Energy Conversion Engineering Conference, vol. 1, IEEE, Piscataway, NJ, 1989, pp. 299-307.

2. Quinn, R.D.; and Yunis, I.: Control/Structure Interactions of Freedom's Solar Dynamic Modules. Proceedings of AIAA Guidance, Navigation and Control Conference, Part 1, AIAA, 1990, pp. 79-88.

3. Strumpf, H.J.; and Coombs, M.G.: Solar Receiver for the Space Station Brayton Engine. ASME Paper 87-GT-252, 1987.

4. Matthews, L.K.; and Mulholland, G.P.: High Temperature-High Flux Material Testing For Solar Flux Applications. Solar Energy, vol. 23, no. 2, 1979, pp. 175-181.

5. Jaffe, L.D.: Solar Tests of Aperture Plate Materials for Solar Thermal Dish Collectors. Solar Energy Eng., vol. 106, no. 4, Nov. 1984, pp. 408-415.

6. Jaffe, L.D.: Solar Tests of Aperture Plate Materials for Solar Thermal Dish Collectors. NASA CR-173462, DOE/JPL-1060-62, 1983.

7. Matthews, L.; and Mulholland, G.P.: High Temperature Materials Study --- For Thermal Insulation In Solar Furnaces. Seminar on Testing Solar Energy Materials and Systems, Institute of Environmental Sciences, Gaithersburg, Md., 1978, pp. 195-200.

8. Wen, L.; and Roschke, J.: Thermal Response Of Solar Receiver Aperture Plates During Sun Walk-Off. ASME Paper 82-HT-33, 1982.

9. Strumpf, H.J.; and Coombs, M.G.: Advanced Heat Receiver Conceptual Design Study: Final Report. NASA CR-180901, 1987, pp. 204-214.

10. Jefferies, K.S.: Concentration of Off-Axis Radiation by Solar Concentrators for Space Power. NASA TM-102052, 1989.

11. Siegel, R.; and Howell, J.R.: Thermal Radiation Heat Transfer, 2nd Ed., Hemisphere Publishing Corp., 1981, p. 288.

12. Boley, B.A., and Weiner, J.H.: Theory of Thermal Stresses. John Wiley & Sons, 1960, p. 278.

13. Banks, B.A., et al.: Simulation of the Low Earth Orbit Atomic Oxygen Interaction With Materials by Means of an Oxygen Ion Beam, NASA TM-101971, 1989, p. 15.

TABLE I. - MATERIAL TEMPERATURE LIMITS

Material	Maximum usage temperature,[a] K	Melting temperature, K
Tungsten	~3100	3683
Graphite	~3100	----
Board insulation	~1500	2033
Nickel	~1325	1728
Haynes 188	~1375	[b]1575

[a]Or maximum temperature at which material property data exist.

[b]Solidus temperature.

TABLE II. - NATURAL FREQUENCIES OF THE FIRST 38 FLEXIBLE MODES

Mode number	Natural frequency, Hz
23	0.07350245
24	.07424994
25	.07574014
26	.07651404
27	.07806754
28	.08882223
29	.09397283
30	.1009129
31	.1027209
32	.1214049
33	.1299069
34	.1330869
35	.1454049
36	.1580439
37	.1605129
38	.1682609
39	.1682809
40-47	.1702689
48	.1846808
49	.2334408
50	.2490278
51	.2966708
52-59	.3175788
60	.3181077

TABLE III. - DOCKING SIMULATION AND CONTROL SUMMARY

	FP bandwidth, Hz	Maximum torque, in.-lb	Maximum off-pointing, deg	Time to 0.1°, sec
Case I	0.5	2500	0.05	0
Case II	.05	1000	.23	30
Case III	.05	250	.34	100

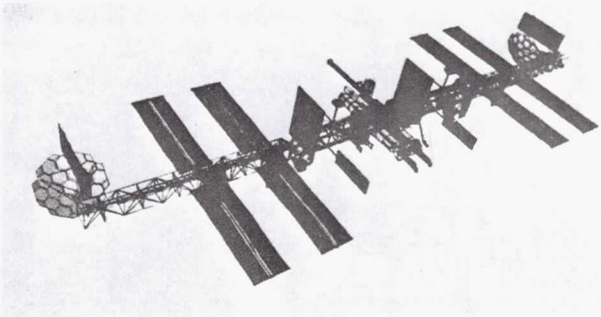

Figure 1.—Space Station Freedom, MB-15 with solar dynamic power modules.

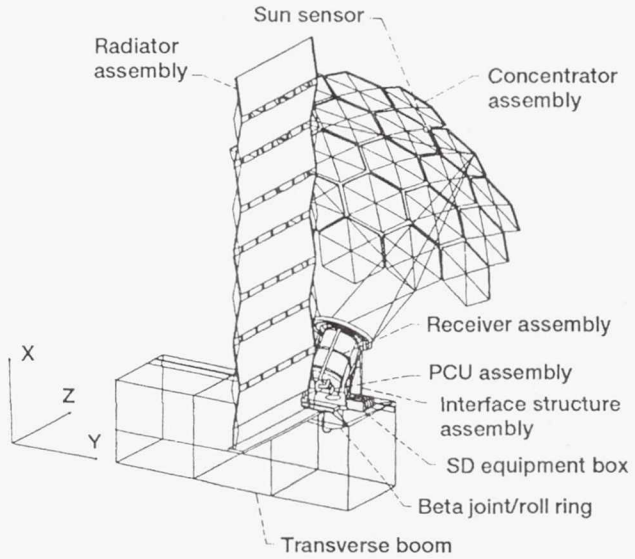

Figure 2.—Solar dynamic power system.

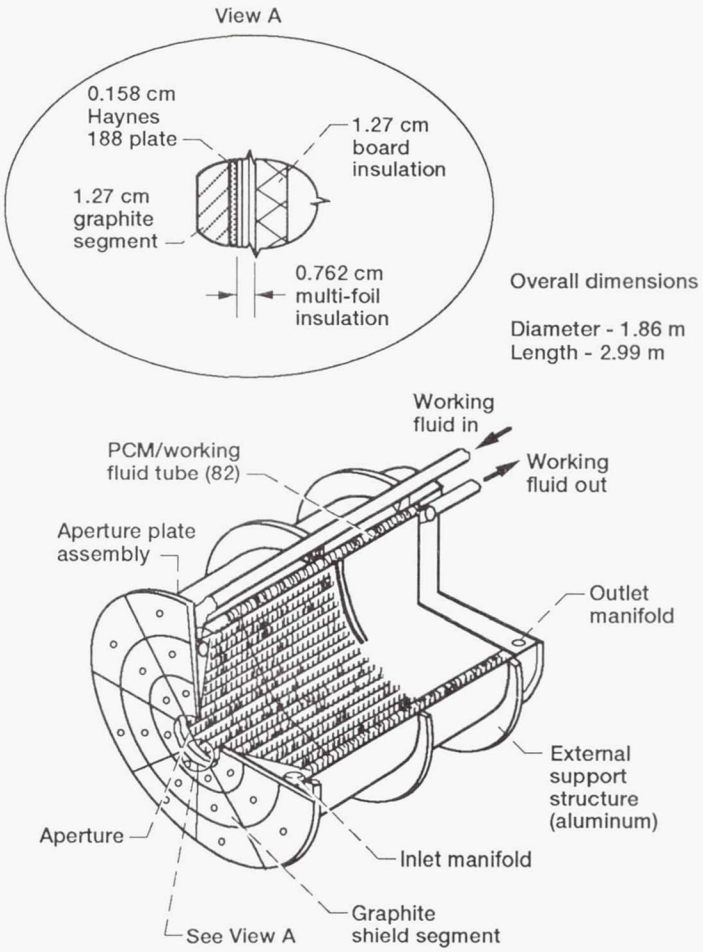

Figure 3.—Solar receiver with aperture plate assembly.

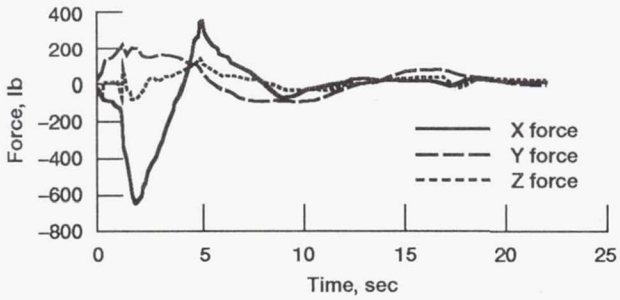

Figure 4.—Shuttle docking forces on station, JSC case 803T.

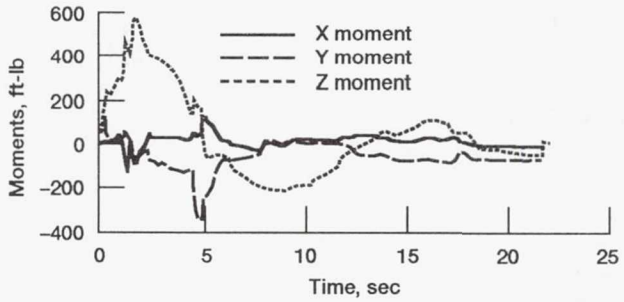

Figure 5.—Shuttle docking moments on station, JSC case 803T.

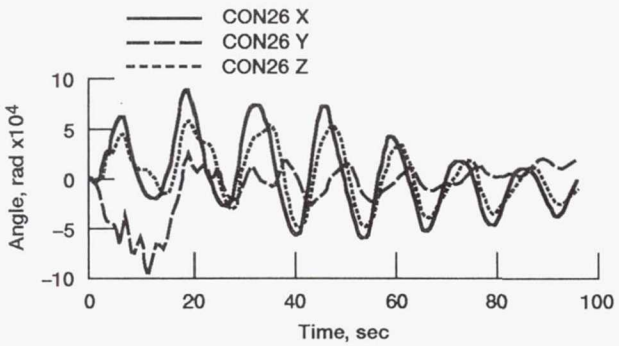

Figure 6.—Starboard concentrator angular motion for case I.

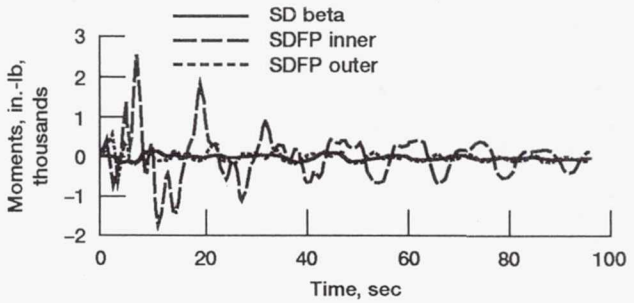

Figure 7.—Beta and fine-pointing gimbal control torques for case I.

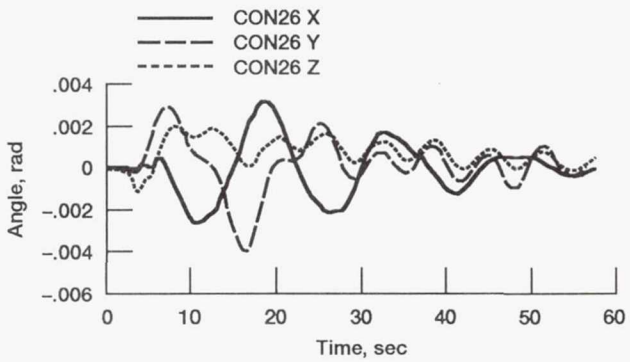

Figure 8.—Starboard concentrator angular motion for case II.

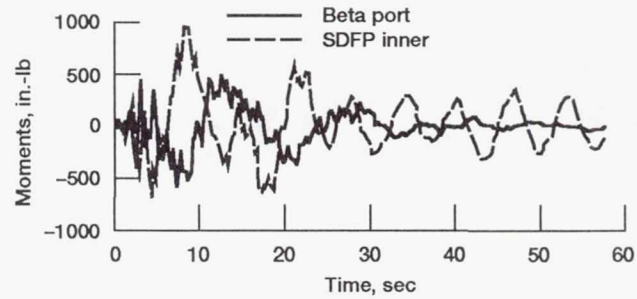

Figure 9.—Beta fine-pointing gimbal control torques for case II.

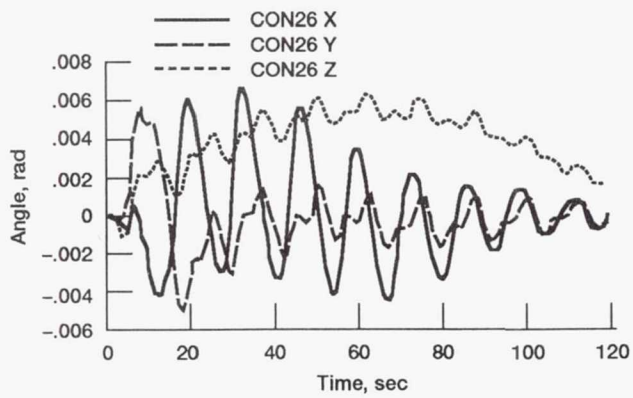

Figure 10.—Starboard concentrator angular motion for case III.

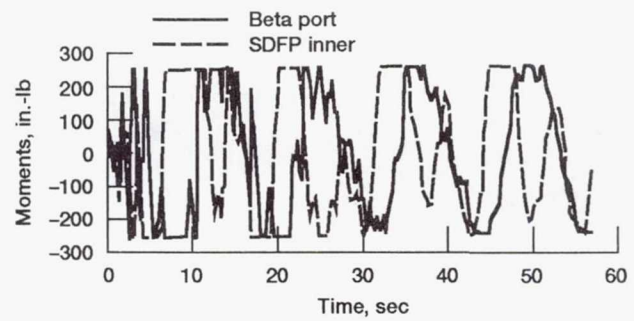

Figure 11.—Beta and fine-pointing gimbal control torques for case III.

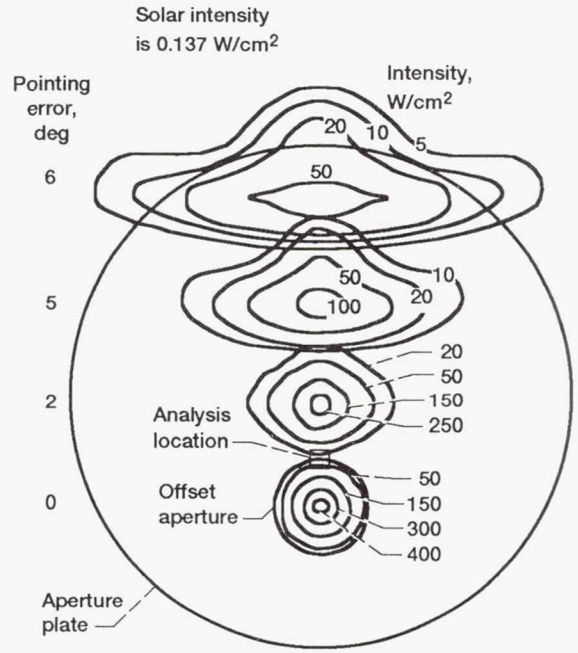

Figure 12.—Aperture plate incident flux versus pointing error [10].

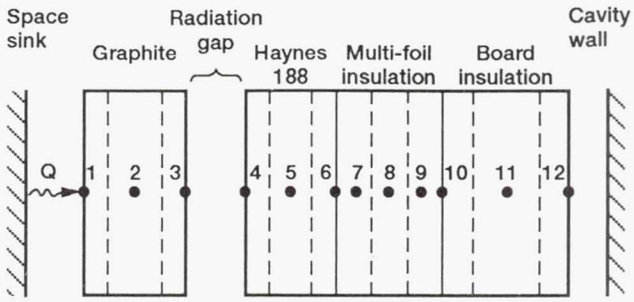

Layer material	Thickness, cm
Graphite	1.270
Haynes 188	.158
Multi-foil insulation	.762
Insulation board	1.270

Figure 13.—Aperture plate finite difference model.

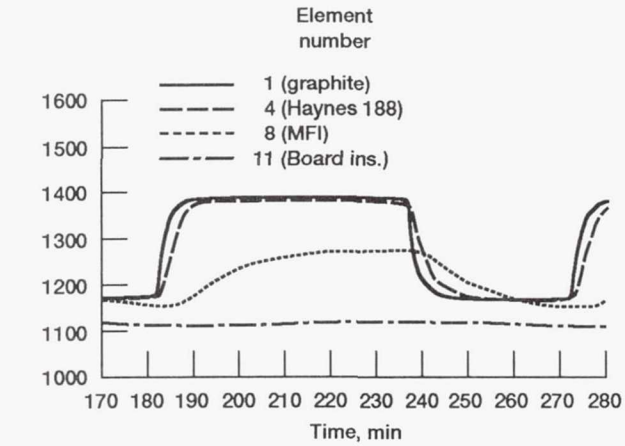

(a) Case I.

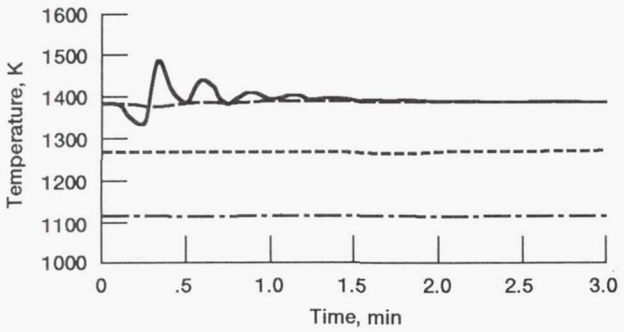

(b) Case II.

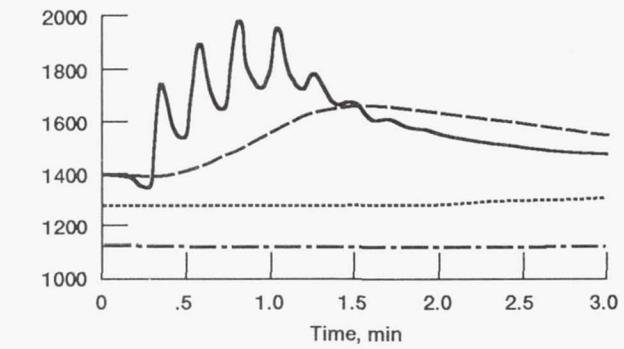

(c) Case III.

Figure 14.—Aperture plate layer temperatures (note changes in ordinate and abscissa scales).

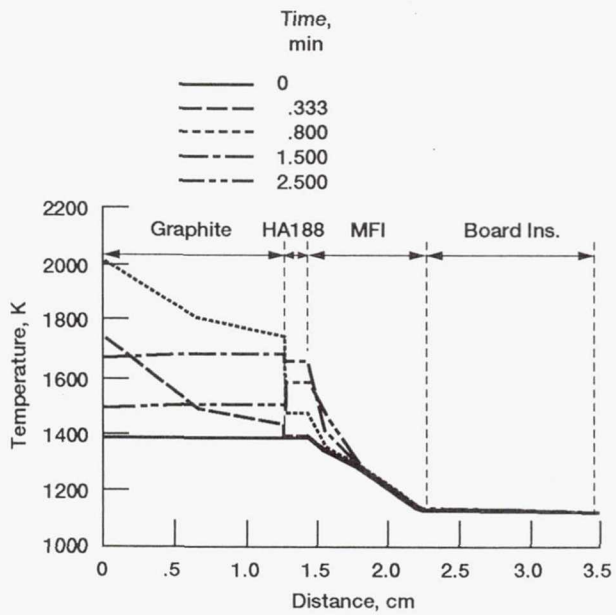

Figure 15.—Case III aperture plate layer temperature gradients.

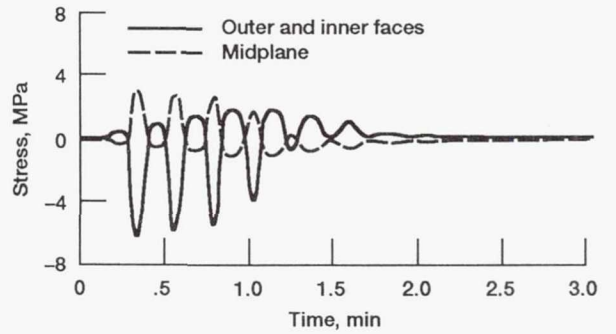

Figure 16.—Case III graphite segment in-plane thermal stresses.

REPORT DOCUMENTATION PAGE

Form Approved
OMB No. 0704-0188

1. AGENCY USE ONLY (*Leave blank*)	2. REPORT DATE	3. REPORT TYPE AND DATES COVERED
		Technical Memorandum

4. TITLE AND SUBTITLE

Solar Dynamic Modules for Space Station Freedom: The Relationship Between Fine-Pointing Control and Thermal Loading of the Aperture Plate

5. FUNDING NUMBERS

WU-474-52-10

6. AUTHOR(S)

Roger D. Quinn and Thomas W. Kerslake

7. PERFORMING ORGANIZATION NAME(S) AND ADDRESS(ES)

National Aeronautics and Space Administration
Lewis Research Center
Cleveland, Ohio 44135-3191

8. PERFORMING ORGANIZATION REPORT NUMBER

E-6109

9. SPONSORING/MONITORING AGENCY NAMES(S) AND ADDRESS(ES)

National Aeronautics and Space Administration
Washington, D.C. 20546-0001

10. SPONSORING/MONITORING AGENCY REPORT NUMBER

NASA TM-104498

11. SUPPLEMENTARY NOTES

Prepared for the International Solar Energy Conference sponsored by the American Society of Mechanical Engineers, Lahaina, Maui, Hawaii, April 5-9, 1992. Roger D. Quinn, Case Western Reserve University, Department of Mechanical and Aerospace Engineering, Cleveland, Ohio 44106 and Summer Faculty Fellow at NASA Lewis Research Center. Thomas W. Kerslake, NASA Lewis Research Center. Responsible person, Thomas W. Kerslake, (216) 433-5373.

12a. DISTRIBUTION/AVAILABILITY STATEMENT

Unclassified - Unlimited
Subject Categories 20 and 39

12b. DISTRIBUTION CODE

13. ABSTRACT *(Maximum 200 words)*

Dynamic simulations of Space Station Freedom configured with SD power modules were performed. The structure was subjected to shuttle docking disturbances, while being controlled with a "natural" vibration and tracking control approach. Three control cases were investigated for the purpose of investigating the relationship between actuator effort, SD pointing and thermal loading on the receiver aperture plate. Transient, one-dimensional heat transfer analyses were performed to conservatively predict temperatures of the multi-layered receiver aperture plate assembly and thermal stresses in its shield layer. Results indicate that the proposed aperture plate is tolerant of concentrated flux impingement during short-lived structural disturbances. Pointing requirements may be loosened and the required control torques lessened from that previously specified. Downsizing and simplifying the joint drive system should result in a considerable savings in mass.

14. SUBJECT TERMS

Space stations; Solar dynamic power systems; Dynamic structural analysis; Pointing control systems; Solar flux; Solar collectors; Heat shielding; High temperature; Thermal stresses

15. NUMBER OF PAGES

20

16. PRICE CODE

A03

17. SECURITY CLASSIFICATION OF REPORT	18. SECURITY CLASSIFICATION OF THIS PAGE	19. SECURITY CLASSIFICATION OF ABSTRACT	20. LIMITATION OF ABSTRACT
Unclassified	Unclassified	Unclassified	